scientific reports

Check for updates

OPEN

lncRNA RP11-199F11.2 promotes high-grade serous ovarian cancer cell proliferation by regulating cuproptosis through FDX1

Shishi Xu[1,2,5], Linping Wang[3,5], Yingying Wu[4], Yufang Xia[1], Lingzhi Wang[1], Xiao Yu[1], Xin Sun[1] & Yanhui Lou[1]✉

To elucidate the expression characteristics of the long noncoding RNA RP11-199F11.2 (RP11) in high-grade serous ovarian cancer (HGSOC) and its potential mechanism of regulating cancer progression via the copper-death pathway, and to evaluate the therapeutic potential of the copper ion carrier ES-Cu. The interaction between RP11 and FDX1 was predicted via bioinformatics; the posttranscriptional inhibition of FDX1 by RP11 was verified via qRT–PCR and Western blotting; the effects of RP11 knockdown/overexpression on proliferation were evaluated in in vitro and in subcutaneous xenograft cancer models; ES-Cu was used to induce copper death, and cell death patterns and circulating inflammatory cytokines were detected via flow cytometry and ELISA. RP11 was significantly highly expressed in HGSOC tissues and was positively correlated with FIGO stage and lymph node metastasis ($P < 0.01$). Mechanistically, bioinformatic analysis suggests that RP11 may binds the 3′-UTR of FDX1 to reduce its translation, thereby limiting copper death and increased cell proliferation. ES-Cu treatment restored FDX1 expression, re-activated copper death, and reduced tumour volume by 68% ($P < 0.001$) without detectable histological toxicity. RP11 is associated with inhibits copper death and modulation of local inflammatory milieu by suppressing FDX1, which may contribute to HGSOC progression. ES-Cu re-activates the FDX1-copper-death axis, providing a potential strategy for combining copper-death induction with immunomodulation in HGSOC.

Keywords High-grade serous ovarian cancer, lncRNA RP11-199F11.2, FDX1, Cuproptosis, Inflammatory microenvironment

The early symptoms of ovarian cancer are often subtle, and the disease is usually diagnosed at an advanced stage[1]. The ten-year survival rate is only approximately 17%, and within 18 months, approximately 80% of patients will relapse and enter a refractory stage[2]. Ovarian cancer is a major threat to women's health worldwide, and 70–80% of epithelial ovarian cancers belong to the high serous subtype (HGSOC), which has the poorest prognosis[3]. The ten-year mortality rate can reach as high as 70%[4]. The identification of its molecular mechanism is urgently needed. Long noncoding RNAs (lncRNAs) play an increasingly important role in cancer regulation[5]; our previous research revealed that the lncRNA RP11-199F11.2 (RP11), located at 17p13.1 and with a full length of 1112 nt, is highly expressed in HGSOC tissues and is positively correlated with lymph node metastasis, the FIGO stage, and increased TP53 activity, suggesting that it may promote cancer progression through an unknown mechanism[6,7].

The proposed mechanism of copper death (cuproptosis) provides insight into the function of RP11 in HGSOC[8]. The core link of this pathway has been clearly identified: the copper ion carrier elesclomol forms a complex (ES-Cu) with $CuCl_2$[9], transporting Cu^{2+} to the mitochondria; mitochondrial ferredoxin-1 (FDX1) catalyses the reduction of Cu^{2+} to Cu^{+} and mediates the sulfenylation of the TCA cycle enzyme DLAT, subsequently triggering protein oligomerization, the disruption of iron-sulfur clusters, and cell death[10,11]. Elevated copper content in cancer tissues is associated with poor prognosis, and the downregulation of FDX1 expression has been confirmed to be associated with resistance in multiple cancers[12,13]. Research has revealed that copper

[1]Department of Gynaecology, The Affiliated Hospital of Qingdao University, Qingdao 266003, China. [2]Qingdao University, Qingdao 266071, China. [3]Weihai Maternal and Child Health Hospital Affiliated to Qingdao University, Weihai 264200, China. [4]Department of Obstetrics and Gynaecology, Shanghai First Maternity and Infant Hospital, Shanghai 201204, China. [5]Shishi Xu and Linping Wang contributed equally to this work. ✉email: louyh@qdu.edu.cn

death can activate dendritic cells and $CD8^+$ T cells by releasing damage-associated molecular patterns (DAMPs), reshaping the immune microenvironment and enhancing anticancer immune surveillance[14,15]; conversely, FDX1 deficiency leads to copper death escape, weakening anticancer immunity and promoting the formation of an immunosuppressive microenvironment[16]. Although ovarian cancer is characterized by high copper levels[17], the expression profile of FDX1 in HGSOC and its regulatory role in the copper death-immune axis have not been elucidated.

Integration of the bioinformatics prediction results and the transcriptome chip results of our research group revealed that the potential target sequence of lncRNA RP11 is complementary to the 3′-UTR of FDX1. Moreover, in HGSOC tissues with high RP11 expression, the FDX1 mRNA level was significantly reduced, suggesting that RP11 may inhibit FDX1 through posttranscriptional regulation. Based on these findings, we hypothesize that the RP11-FDX1 axis can block the copper death pathway, alter local inflammatory cytokine levels and confer copper tolerance advantages to cancer cells.

We speculate that RP11 may inhibit the copper death pathway by suppressing FDX1, thereby protecting HGSOC cells from copper toxicity and promoting the continuous proliferation of cancers. This study is the first to connect a long non-coding RNA (RP11) to cuproptosis in high-grade serous ovarian cancer, offering a non-mutation-driven perspective on therapy resistance. Therefore, this study first confirmed that RP11 is highly expressed in HGSOC tissues, whereas FDX1 is expressed at low levels; functional experiments further revealed that RP11 significantly promotes the proliferation of ovarian cancer cells both in vitro and in vivo. More importantly, ES-Cu pulse therapy can downregulate RP11 and restore FDX1 expression, reactivating the copper death mechanism and significantly inhibiting cancer growth. These findings link RP11, FDX1, and the copper death mechanism organically, providing a new theoretical basis and intervention strategies for the diagnosis and targeted treatment of HGSOC.

Materials and methods

Tissue specimens

Thirty HGSOC tissue samples from patients who underwent surgical treatment at the Affiliated Hospital of Qingdao University from September 2021 to June 2023 were collected. The patients whose diagnosis was confirmed by postoperative pathological examination did not receive radiotherapy or chemotherapy before surgery. Twenty-six normal fallopian tube tissue samples from patients who underwent total hysterectomy with bilateral adnexectomy for uterine fibroids during the same period were collected as controls. Fresh tissue samples were immediately stored in an ultralow-temperature freezer until use. The study methodologies were approved by the Medical Ethics Committee of the Affiliated Hospital of Qingdao University and conformed to the standards set by the Declaration of Helsinki (QYFY WZLL 30,704).

Cell culture

We purchased the OVCAR3 and HO8910 cell lines from the American Culture Collection. STR authentication and mycoplasma testing were performed every 3 months (last tested May 2024); cells were used within 10 passages.OVCAR3 and HO8910 cells were cultured in complete culture medium supplemented with Dulbecco's modified Eagle's medium (Meilune, Dalian, China), foetal bovine serum (Procell, Wuhan, China) and penicillin–streptomycin solution (Procell, Wuhan, China) in a 5% CO_2 and 37 °C incubator.

Lentiviral transduction

The lentiviral vectors (LV-RP11-RNAi-1/2 and LV-RP11) were obtained from Genechem (Shanghai, China). RP11-knockdown and -overexpressing cells were generated via transduction via lentiviral vectors, and the cells were divided into 5 groups: sh-NC, sh-RP11-1, sh-RP11-2, p-NC and p-RP11. After being seeded in 6-well plates, the cells (1×10^5) were cultured for 24 h to reach a density of approximately 30%. The lentiviruses were transduced into OVCAR3 and HO8910 cells with HitrsnsG P virus transduction reagent (Genechem, Shanghai, China). The transduction medium was replaced with fresh complete culture medium 16 h later. The transduction efficiency was assessed by fluorescence microscopy after 72 h.

Quantitative real-time PCR (qRT–PCR)

Total RNA was extracted from tissues and cells with RNA Easy (Vazyme, Nanjing, China). A qRT-PCR Assay Kit (ABclonal, Wuhan, China) was used for both RNA reverse transcription and real-time PCR. Gene expression was subsequently determined via a fluorescence quantitative PCR instrument (Roche480, Basel, Switzerland). We used the $2^{-\Delta\Delta Ct}$ method to calculate the relative RNA levels. The specific primers used are shown in Table 1.

Western blot analysis

RIPA lysis buffer (Elabscience, Wuhan, China) was used to collect total intracellular protein, and a BCA protein assay kit (Meilune, Dalian, China) was used to measure the protein concentration. Western blotting

Gene name	Forward primer (5'–3')	Reverse primer (5'–3')
RP11	CATCTCTTAGCTCGCGCGGTTGT	CGTAAGTACGGCACAAAGTGG
FDX1	TGGGCTGCCAAATCTGTTTGA	ATTGTCTGGCATCAGCCACTG
β-actin	GGGAGACGTGCGTGACATT	GGAACCGCTCATTGCCAAT

Table 1. Primer sequences.

was conducted via electrophoresis and a blotting system (Bio-Rad, California, USA). Protein samples were separated by SDS-PAGE and electrotransferred to PVDF membranes (Millipore, Massachusetts, USA). Primary antibodies against FDX1 (1:1500, A20895, ABclonal, Wuhan, China) and β-actin (1:1500, GB11001, Servicebio, Wuhan, China) were incubated with the membranes overnight at 4 °C after blocking for 2 h. The membranes were incubated with a goat anti-rabbit IgG-HRP antibody (1:10,000, abs20040ss, Absin, Shanghai, China) for 1 h the following day. Finally, immunoreactivity was detected via a chemiluminescence imaging analyser (Vilber-Lourmat, Paris, France).

Cell proliferation assay

After a total of 3×10^3 cells were seeded in triplicate into 96-well plates, a Cell Counting Kit-8 (CCK-8; Tsbiochem, Shanghai, China) was added to the wells at 24, 48, 72, and 96 h. The cells were incubated for 2 h. We measured the absorbance at 450 nm (OD450) via a microplate reader (TECAN, Canton, Switzerland) to determine cell viability.

Colony formation assay

The cells were seeded in 6-well plates at a density of 1000 cells per well and cultured for 14 days. After being washed with PBS, the cells were fixed with paraformaldehyde (Servicebio, Wuhan, China) for 20 min and then stained with crystal violet ammonium oxalate solution (Solarbio, Beijing, China) for 30 min, after which the cells were photographed.

Half-maximal inhibitory concentration (IC50) assay

A total of 5×10^3 cells were seeded in 96-well plates and pulse-treated with 0, 20, 40, 80, 120, or 160 nM elesclomol (supplemented with or without 1 μM $CuCl_2$) for 2 h. After culturing for 24 h, cell viability was examined via a CCK-8 assay. TTM was used at 10 μM according to Kuang et al., 2025, to achieve selective copper chelation.

Pyruvate dehydrogenase (PDH) activity assay

A total of 1×10^6 cells were added to 200 μl of extraction solution. The reagents and supernatant were added to the standard wells, control wells and determination wells. OD values at 450 nm were measured for 20 s, 3 min and 20 s in each well. A standard fitting curve was drawn, and the PDH activity of each sample was calculated according to the measured protein concentration.

Flow cytometry

A total of 5×10^5 cells in good condition were collected and assessed with an apoptosis detection kit (Yeasen, Shanghai, China). After resuspension with binding buffer, 10 μl of PI and 5 μl of Annexin V-FITC were added to the cells, followed by incubation for 15 min in the dark. Finally, flow cytometry was used to detect apoptosis.

Haematoxylin and eosin (H&E) and immunohistochemical analysis

The tumour tissue was embedded in paraffin wax and cut into 5 μm thick sections. For H&E staining, the tissue sections were dewaxed and stained with a standard H&E solution. For immunohistochemical staining, tissue sections were dewaxed, and antigen retrieval was performed in citrate buffer by heating in a boiling water bath (100 °C) in a microwave oven for 10 min. Endogenous peroxidase activity was blocked by incubation with 3% H2O2 for 10 min at room temperature. The paraffin wax sections were incubated with the primary antibody at 4 °C overnight and then with a goat anti-mouse IgG-HRP antibody (1:200, GB23301, Servicebio, Wuhan, China) at room temperature for 50 min. After haematoxylin restaining, the sections were dehydrated and sealed. The staining results were observed via an optical microscope.

Tumour xenograft model

BALB/c-nude female mice (five weeks old) were purchased from Jinan Pengyue Laboratory Animal Breeding Co., Ltd. (China) and were fed in an SPF-grade laboratory. The mice were randomly divided into eight groups (n = 8): NC, NC + ES-Cu, sh-RP11, sh-RP11 + ES-Cu, p-NC, p-NC + ES-Cu, sh-RP11 + p-RP11, and sh-RP11 + p-RP11 + ES-Cu. OVCAR3 cells (5×10^7/mouse) transduced with lentiviral vectors were mixed with Matrigel (ABW, Shanghai, China) and then injected into the right flanks of the mice within 1 h. After tumour formation, body weight and tumour length and width were measured every 3 days. The calculation formula for tumour volume was as follows: tumour volume (mm^3) = [length (mm) × width $(mm)^2$]/2. Mice were euthanized by cervical dislocation under isoflurane anesthesia (4% induction, 2% maintenance) at the end of the experiment or when humane endpoints were reached (≥ 20% body weight loss or tumor volume > 1,000 mm^3).

Animal experiment details: mice were randomized by body weight (block design); tumour measurements were performed by an investigator blinded to group allocation. The study used n = 3 mice per group (power calculation based on pilot data, α = 0.05, power ≥ 80%). Mice were removed if body-weight loss exceeded 20% or tumour volume > 1,000 mm^3; no animals were excluded from final analyses. ES-Cu was administered as 80 nM elesclomol + 1 μM $CuCl_2$ by intraperitoneal injection every 72 h for 3 weeks. Individual tumor measurements (length and width in mm), final tumor weight (g), and animal body weight (g) are provided in Supplementary Table S1.

All animal procedures were conducted in accordance with the ARRIVE guidelines (Animal Research: Reporting of In Vivo Experiments) and the ethical standards of our institution, The experiments involving animals were authorized by the Animal Experiment Ethics Review Committee of the Affiliated Hospital of Qingdao University(AHQU-MAL20230616) .

TdT-mediated dUTP nick end labelling

The tissue sections were successively put into xylene Ⅰ, Ⅱ and Ⅲ for 10 min at each step, and the paraffin was removed. The mixture was then successively incubated in absolute ethanol solutions I, II and III for 5 min, after which it was finally washed with distilled water. The slices were immersed in proteinase K solution and incubated at 37 °C for 10–15 min to increase their permeability. The sections were washed three times with PBS for 5 min each. The sections were immersed in TUNEL reaction solution and incubated at 37 °C for 60 min in the dark. The sections were washed three times with PBS again. The sections were immersed in DAPI staining solution and stained in the dark at room temperature for 5 min to stain the nuclei blue. The samples were washed and dried, the samples were sealed, and the staining results were observed under a fluorescence microscope.

Enzyme-linked immunosorbent assay

In accordance with the experimental requirements, samples (plasma, cell culture supernatant, etc.) were collected and processed to ensure that the samples were free of haemolysis and contamination. The standard in the ELISA kit was diluted into a series of concentration gradients (such as 0, 1, 2, 4, 8, and 16 ng/ml) as the control of the standard curve. The standard and sample were added to 96-well ELISA plates at 100 μl per well, and duplicate wells were set up. The mixture was incubated at 37 °C for 30 min in the dark. The samples were washed with PBS and shaken dry. The enzyme-labelled antibody (100 μl per well) was added, and the mixture was incubated at 37 °C for 30 min in the dark. The samples were washed and dried again. The substrate mixture (100 μl per well) was added, and the mixture was incubated at 37 °C for 15 min in the dark. The termination mixture (50 μl per well) was added, and the reaction was stopped. The absorbance value of each well was measured at a wavelength of 450 nm with a microplate reader. The concentrations of immune factors in the samples were calculated according to the standard curve for statistical analysis.

Statistical analysis

We used GraphPad Prism statistical software to perform the statistical analyses. A t test or one-way ANOVA was used to compare the data between or among groups, respectively. Each experiment was repeated three times, and the data are presented as the mean ± sd. $P < 0.05$ was considered to indicate statistical significance.

Results

RP11 is upregulated in ovarian cancer cells and promotes their proliferation

To verify the expression of RP11 in HGSOC tissues, we conducted qRT-PCR analysis. The results revealed that the expression of RP11 in HGSOC tissues was greater than that in normal fallopian tube tissues (Fig. 1A). To confirm the high expression trend of RP11 in HGSOC tissues, we analysed the expression of RP11 in the IOSE80, A2780, HO8910, OVCAR3 and SKOV3 cell lines via qRT-PCR (Fig. 1B). HO8910 and OVCAR3 cells were selected because their RP11 levels and TP53/BRCA2 mutation profiles were the closest to those of primary HGSOC, thus serving as representative models for functional studies. To further verify the function of RP11 in ovarian cancer, we transfected lentiviral vectors into HO8910 and OVCAR3 cells to regulate the expression of RP11. The expression of the fluorescent protein after transfection was observed via fluorescence microscopy, as shown in Fig. 1C. The transfection efficiency was verified by qRT-PCR (Fig. 1D,E). The CCK-8 assay results indicated that the presence of RP11 significantly increased cell viability; conversely, the reduction in RP11 levels significantly inhibited cell viability (Fig. 1F,G). Additionally, a colony formation assay was used to evaluate cell proliferation. The results revealed that the number of colonies formed by OVCAR3 and HO8910 cells transduced with p-RP11 was greater than that formed by cells transduced with p-NC (Fig. 1H); moreover, the number of colonies formed by OVCAR3 and HO8910 cells transduced with sh-RP11-1 and sh-RP11-2 was significantly lower than that formed by cells transduced with sh-NC (Fig. 1I). We also collected data on age, FIGO stage, lymph node status, CA125, and TP53 mutations from 56 patients (Table 2). We considered that RP11 was highly expressed in HGSOC tissues and positively correlated with FIGO stage and lymph node metastasis ($P < 0.01$).

RP11 regulates ovarian cancer cells by downregulating FDX1

To investigate the downstream proteins of RP11, we screened the LncRRIsearch database and found that there was a binding target between RP11 and FDX1 (Fig. 2A). This interaction remains largely supported by bioinformatics predictions, and further experimental evidence is needed to consolidate its direct binding characteristics. We evaluated the expression of FDX1 in HGSOC tissues via Western blotting. The results revealed that the expression level of FDX1 in HGSOC tissues was significantly lower than that in normal fallopian tube tissues (Fig. 2B). To verify whether FDX1 is regulated by RP11, we conducted Western blotting assays. As shown in Fig. 2C,D, RP11 knockdown upregulated the protein expression of FDX1 but did not change the FDX1 mRNA level (Supplementary Figure S1); this finding indicates that its regulatory mechanism is posttranscriptional rather than transcriptional.

ES-Cu promotes copper-dependent cell death via the RP11/FDX1 axis

The IC50 value of ES-Cu was determined via the CCK-8 assay. We concluded that when the CuCl2 concentration in the culture medium was 1 μM, the IC50 value in OVCAR3 cells was 78.19 nM and that in HO8910 cells was 79.6 nM (Fig. 3A,B). For ease of operation, 80 nM elesclomol was used for pulse treatment in the subsequent experiments. To determine the mode of cell death induced by ES-Cu, the cells were pretreated with Z-VAD-FMK, necrostatin-1, ferrostatin-1, chloroquine (CQ), or tetra thiomolybdate (TTM). TTM partially reversed the cytotoxicity induced by ES-Cu, while the inhibition of caspases did not (Fig. 3C). These findings indicate that the mechanism is dependent on copper rather than simple apoptosis. qRT-PCR and Western blotting confirmed that ES-Cu reduced the expression of RP11 and upregulated FDX1 (Fig. 3D–F). Flow cytometry revealed that the cells were Annexin V/PI positive (Fig. 3G), which was consistent with early membrane damage during copper-

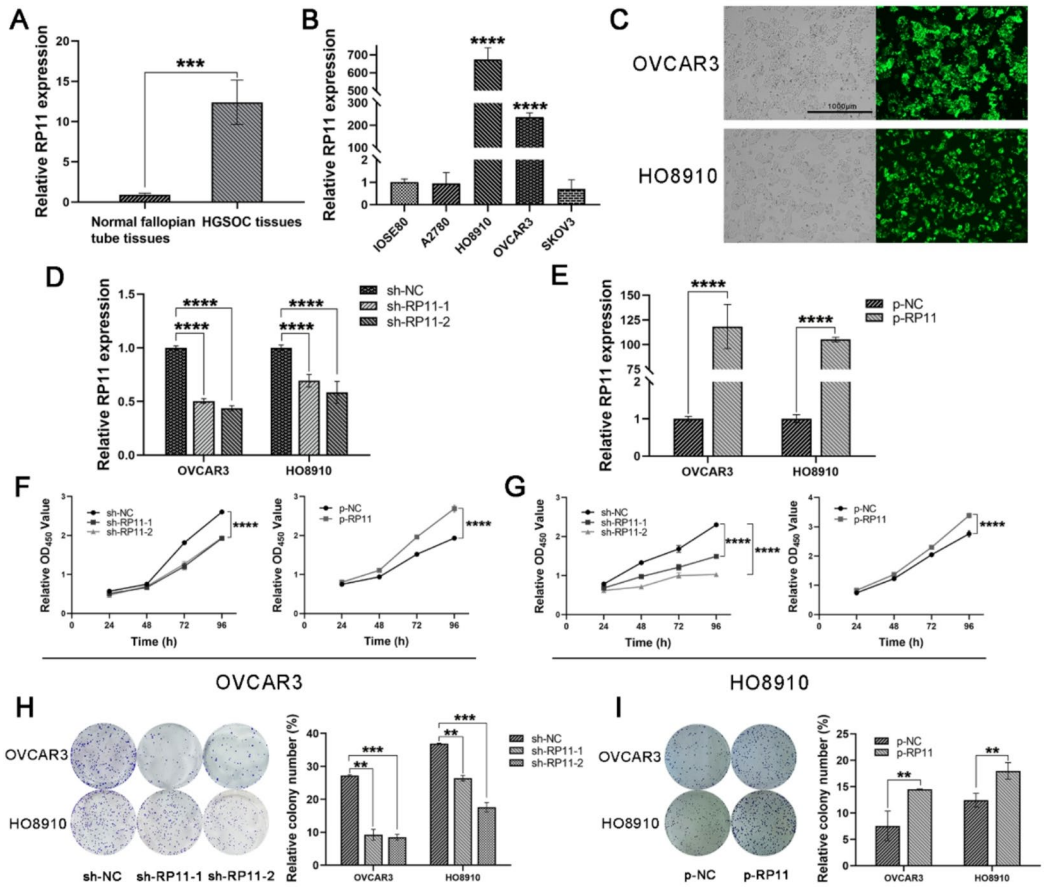

Fig. 1. RP11 is upregulated in ovarian cancer cells and promotes their proliferation. (**A**) RP11 expression in HGSOC tissues and normal fallopian tube tissues was compared via qRT-PCR. (**B**) The two most appropriate cell lines were selected from among the five cell lines for subsequent experiments. (**C**) Fluorescent protein expression after cells were transduced with lentivirus for 72 h (scale bars, 1000 μm). (**D**) RP11 expression in cells transduced with the LV-RP11 lentivirus significantly increased. (**E**) RP11 expression after RP11 knockdown via lentivirus. (**F**,**G**) In OVCAR3 and HO8910 cells, RP11 overexpression promoted cell proliferation, and RP11 silencing suppressed cell proliferation. H: Colony formation increased in ovarian cancer cells overexpressing RP11. I: RP11 knockdown inhibited colony formation. (**$P < 0.01$; ***$P < 0.001$; ****$P < 0.0001$). Data are presented as mean ± SD with 95% confidence intervals for pairwise differences; Bonferroni post-hoc correction was applied and adjusted *P* values are indicated in the figure.

Variable	HGSOC (n = 30)	Normal (n = 26)	*P* value
Age (years)	58.3 ± 7.2	56.8 ± 8.0	0.47
FIGO stage (III/IV)	24 (80%)	–	–
Lymph node metastasis	18 (60%)	0 (0%)	< 0.001**
CA125 (U/ml)	742 (353–1215)	21 (14–29)	< 0.001**
TP53 mutation	25 (83%)	–	–

Table 2. Baseline clinical characteristics of the study cohort. Multivariable logistic regression showed that high RP11 expression was independently associated with advanced FIGO stage (OR = 3.52, 95% CI 1.14–10.91, $P = 0.029$, adjusted for age, CA125 and TP53 mutation).

induced cell death; While DLAT oligomerization, mitochondrial Cu deposition and Fe–S cluster integrity—gold-standard markers of cuproptosis—remain to be examined in follow-up work, the present data support a Cu-dependent death mode. Bonferroni-corrected *P* values are listed in Fig. 3G.

RP11 promotes the proliferation of ovarian cancer cells in vivo

To determine the function of RP11 in vivo, we injected OVCAR3 cells transfected with lentiviral vectors into nude mice to establish a cancer subcutaneous xenograft model and then evaluated cancer formation. The expression of

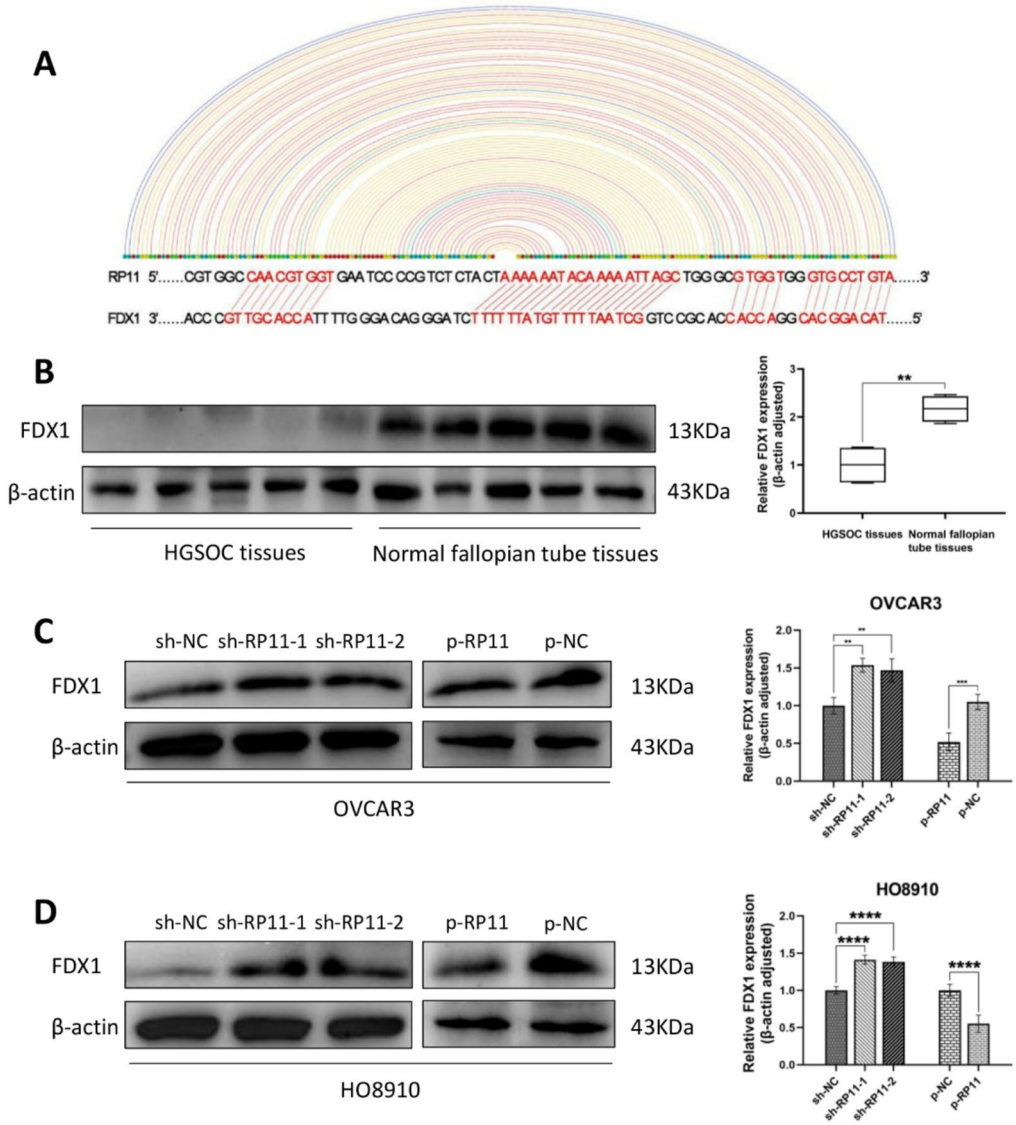

Fig. 2. RP11 regulates ovarian cancer cells by downregulating FDX1. (**A**) A database identified FDX1 as a downstream protein of RP11. (**B**) FDX1 expression was notably lower in HGSOC tissues than in normal fallopian tube tissues. (**C**,**D**) FDX1 protein expression under RP11 knockdown or overexpression in both the OVCAR3 and HO8910 cell lines. (**$P < 0.01$; ***$P < 0.001$; ****$P < 0.0001$). Although the change in FDX1 protein is statistically significant, the magnitude is limited and may reflect a slight translational adjustment; the experiment was repeated n = 3 independent. Data are presented as mean ± SD with 95% confidence intervals for pairwise differences; Bonferroni post-hoc correction was applied and adjusted *P* values are indicated in the figure.

RP11 in xenograft cancer tissues was detected via qRT-PCR. The results revealed that the expression of RP11 was significantly decreased in the Sh-1/2 group but significantly increased in the OE group (Fig. 4A). Representative images of excised tumors from each group are shown (Fig. 4B). The expression level of RP11 significantly affected the proliferation and apoptosis of ovarian cancer cells in a xenograft cancer model in nude mice. Compared with those in the NC group, the cancer formation rate in the RP11-knockdown group was significantly lower, the volume and weight of the transplanted tumours were significantly lower ($P < 0.05$), and the apoptosis rate was significantly greater ($P < 0.05$) (Fig. 4D,F,G). In contrast, the growth rate of the transplanted cancers in the RP11-overexpressing group was significantly accelerated, the volume and weight of the transplanted cancers were significantly increased ($P < 0.05$), and the apoptosis rate was significantly decreased ($P < 0.05$), indicating that RP11 can significantly promote the proliferation of ovarian cancer cells in the body (Fig. 4C,G). Additionally, we further overexpressed RP11 in the RP11-knockdown cell group and found that the cancer growth rate was restored, which further confirmed the role of RP11 in promoting cancer occurrence and development in the body (Fig. 4E). Moreover, after each experimental group was treated with the copper-induced cell death agent ES-Cu (elesclomol and the $CuCl_2$ complex, with a $CuCl_2$ concentration of 1 μm), the growth of the transplanted cancer

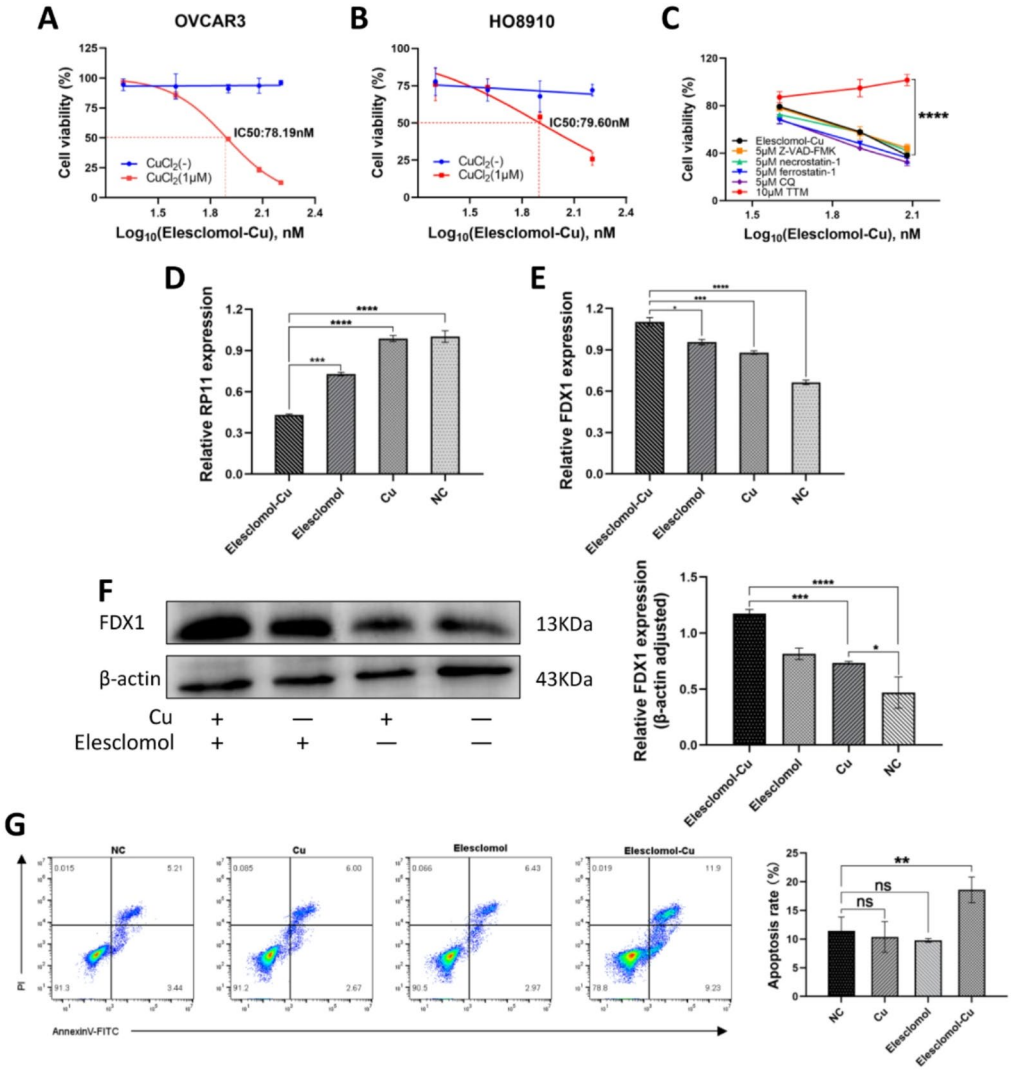

Fig. 3. ES-Cu promotes cuproptosis in ovarian cancer cells by regulating the RP11/FDX1 axis. (**A**,**B**) OVCAR3 and HO8910 cells were pulse-treated with different concentrations of elesclomol (with or without 1 μM $CuCl_2$ in medium) for 2 h, and the CCK-8 assay was used to establish the IC50 of ES-Cu. (**C**) Ovarian cancer cells were pretreated with 5 μM Z-VAD-FMK, 5 μM necrostatin-1, 5 μM ferrostatin-1, 5 μM CQ, or 10 μM TTM for 24 h, and the CCK-8 assay was used to analyse cell viability after pulse treatment with ES-Cu. (**D**) RP11 expression significantly decreased after 2 h of ES-Cu pulse treatment. (**E**) FDX1 mRNA expression was measured via qRT-PCR. (**F**) After ovarian cancer cells were pulse-treated with ES-Cu for 2 h, FDX1 levels increased, as determined by Western blotting. (**G**) Annexin V^+/PI^+ cell death rate (general cell death from early to late stages) increased after ES-Cu pulse treatment, as measured by flow cytometry. (*$P<0.05$; **$P<0.01$; ***$P<0.001$; ****$P<0.0001$). Data are presented as mean ± SD with 95% confidence intervals for pairwise differences; Bonferroni post-hoc correction was applied and adjusted P values are indicated in the figure.

cells in all the groups was significantly inhibited, and the apoptosis rate increased ($P<0.05$). These data support the conclusion that ES-Cu inhibits cancer growth through a copper-dependent mechanism (Fig. 4C,D,E,F,G). The experiments involving animals were authorized by the Animal Experiment Ethics Review Committee of the Affiliated Hospital of Qingdao University (AHQU-MAL20230616) .

Effects of RP11 on the expression of genes related to cuproptosis

The immunohistochemical results revealed that RP11 might inhibit the expression of copper death-related genes (FDX1, DLD) and immune checkpoint PD-L1 through transcriptional regulation and epigenetic modification, thereby downregulating copper ion metabolism and the copper death process and subsequently affecting the cancer microenvironment and local inflammatory milieu . Specifically, in the RP11 knockdown group, the expression of FDX1, DLD, and PD-L1 was significantly upregulated ($P<0.05$), whereas in the RP11 overexpression group, the expression of these genes was significantly downregulated ($P<0.05$) (Fig. 5).In contrast to the copper death-related genes, the copper death-inhibiting gene PDK4 exhibited decreased expression in the RP11-knockdown group and increased expression in the RP11-overexpressing group (Fig. 5). Furthermore,

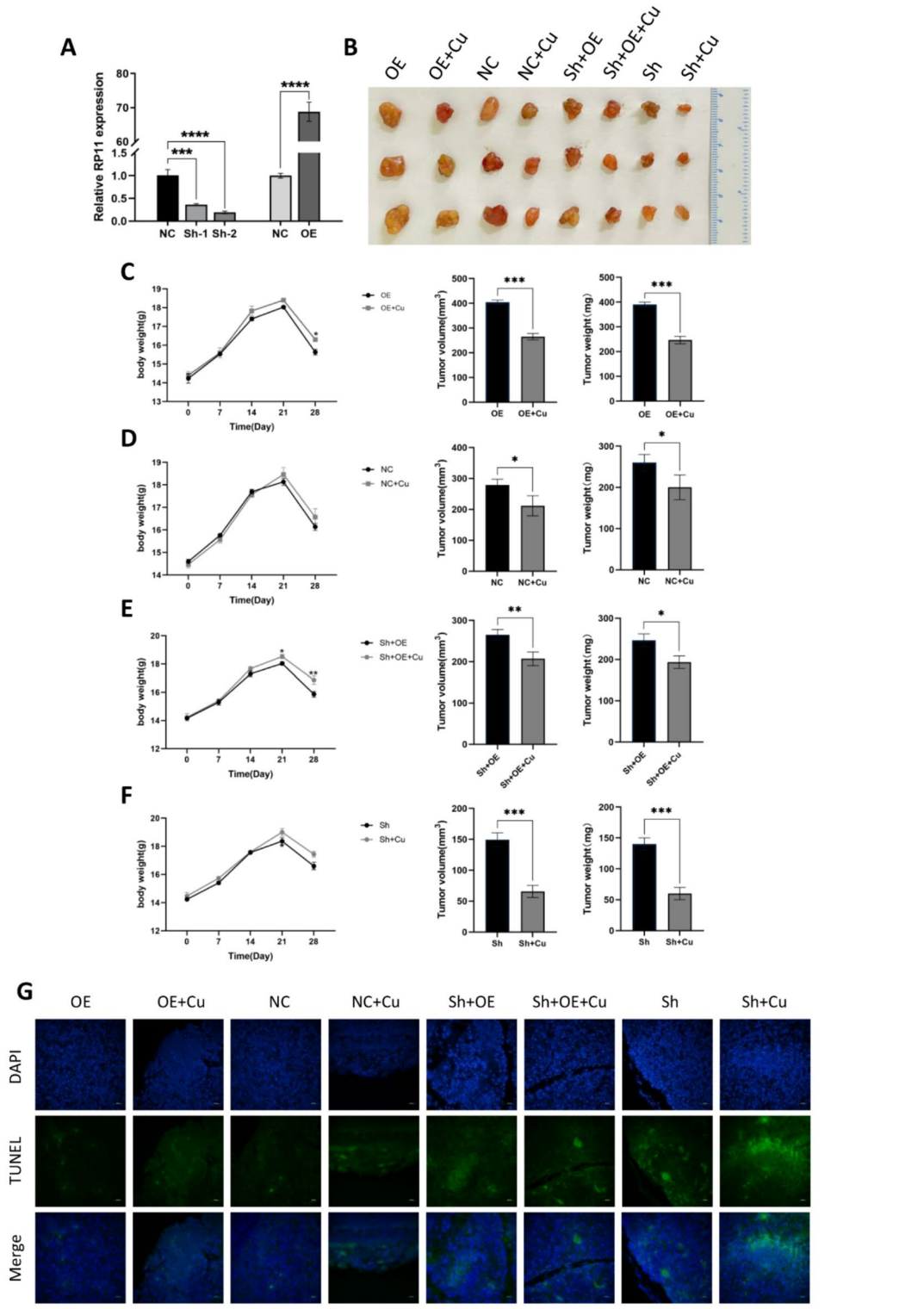

Fig. 4. RP11 promotes the proliferation of ovarian cancer cells in vivo (**A**): RP11 expression in xenograft tumours detected via qRT-PCR. (**B**): Xenograft tumours formed in nude mice from each group. (**C**): Changes in weight, xenograft tumour weight and volume of the rats in the OE group and OE + Cu group. (**D**): Changes in weight, xenograft tumour weight and volume of the rats in the NC group and NC + Cu group. (**E**): Changes in weight, xenograft tumour weight and volume of the rats in the Sh + OE group and Sh + OE + Cu group. (**F**): Changes in weight, xenograft tumour weight and volume of the rats in the Sh group and Sh + Cu group. (**G**): Changes in the level of apoptosis in each group. (*$P < 0.05$; **$P < 0.01$; ***$P < 0.001$; ****$P < 0.0001$). Data are presented as mean ± SD with 95% confidence intervals for pairwise differences; Bonferroni post-hoc correction was applied and adjusted P values are indicated in the figure.

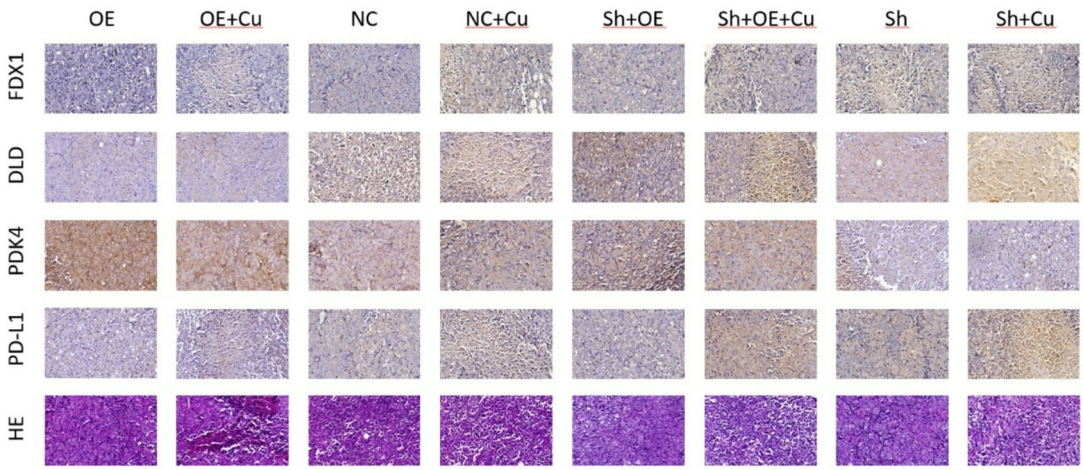

Fig. 5. Effects of RP11 on the expression of genes related to cuproptosis.

after RP11 expression was supplemented in RP11-knockdown cells, the levels of copper death-related genes decreased, whereas the expression of PDK4 increased, indicating that RP11 has a systematic reverse regulatory effect on copper death-related genes.

RP11 regulates the copper death–inflammation axis to reconstruct the immune microenvironment and assess the safety of ES-Cu

Furthermore, the regulation of copper death-related genes by RP11 may also affect local cytokine levels by reshaping the cancer microenvironment (TME). The TME is composed of cancer cells, immune cells, the extracellular matrix, etc., and is an important stage in cancer occurrence and development. By inhibiting FDX1 and the copper death pathway, RP11 lowered plasma IL-6 and IL-8 levels (Fig. 6A,B); whether this reflects reduced DAMPs awaits direct quantification.To further verify the impact of copper-induced death on the immune microenvironment, we conducted further experiments on the key immune factors IL-6 and IL-8, which mediate the activation and migration of immune cells. ELISAs revealed that the plasma levels of IL-6 and IL-8 in RP11-knockdown mice were significantly increased ($P < 0.05$), whereas those in the RP11-overexpressing group were significantly decreased ($P < 0.05$) (Fig. 6A,B). After RP11 was replenished in RP11-knockdown cells, the levels of IL-6 and IL-8 decreased accordingly, suggesting that the RP11-FDX1-copper death axis may affect the activity of immune cells andlocal inflammatory cytokine balance by regulating inflammatory factors.

To comprehensively evaluate the safety of ES-Cu combined therapy, we performed HE staining on the main organs of the experimental mice (heart, liver, spleen, lung, and kidney) (Fig. 6C). The results revealed no obvious pathological changes in any of the experimental groups, suggesting that the toxicity of ES-Cu is controllable at the experimental dose.

Discussion

Once ovarian cancer progresses to the advanced stage, the five-year survival rate is less than 30%, with over 70% being the HGSOC[18]. The “gold standard” regimen of platinum combined with paclitaxel still fails to prevent drug resistance and recurrence in the presence of multiple combined mutations, such as TP53 mutations and HR deficiencies, suggesting the urgent need for new molecular classifications and targeted strategies[19–21]. This study is the first to directly link the lncRNA RP11 with cuproptosis, providing a "nonmutation-driven" perspective on this predicament: RP11 inhibits FDX1 through posttranscriptional regulation and blocks the reduction of copper ions in mitochondria and the sulfenic acidylation of DLAT, thereby inhibiting the oligomerization of copper-dependent proteins and ultimately escaping cuproptosis and maintaining cancer proliferation. Notably, this escape is not simply antiapoptotic but rather a "full-chain" blockade of a novel type of programmed cell death[22]; its downstream effects include not only mitochondrial dysfunction but also a reduction in damage-related molecular patterns (DAMPs)[23], such as mitochondrial ROS, mtDNA, and HMGB1. Modulating local inflammatory cytokine levels, a hypothesis that awaits direct DAMP quantification in immunocompetent models.

As the "rate-limiting enzyme" for copper death, FDX1 is expressed at a relatively low level in various solid cancers[24,25].Our experiments revealed that RP11 forms a stable RNA–RNA complex with the 3′-UTR of FDX1, suggesting a mRNA-masking mechanism by which lncRNAs can directly occlude target transcripts independent of the canonical miRNA-sponge pathway[26,27].This discovery provides insight into the paradigm by which lncRNAs regulate copper homeostasis. Validation of direct binding will be required to confirm the predicted interaction. Additionally, there is still controversy regarding the intersection of copper death, iron death, apoptosis, and necrosis[28]. In this study, the copper chelator TTM could partially reverse the cell death induced by ES-Cu, whereas the pancaspase inhibitor Z-VAD-FMK was ineffective, preliminarily ruling out the dominant role of classical apoptosis; however, gold standard images of DLAT oligomerization and mitochondrial copper deposition have not yet been obtained, suggesting that subsequent studies need to introduce live cell

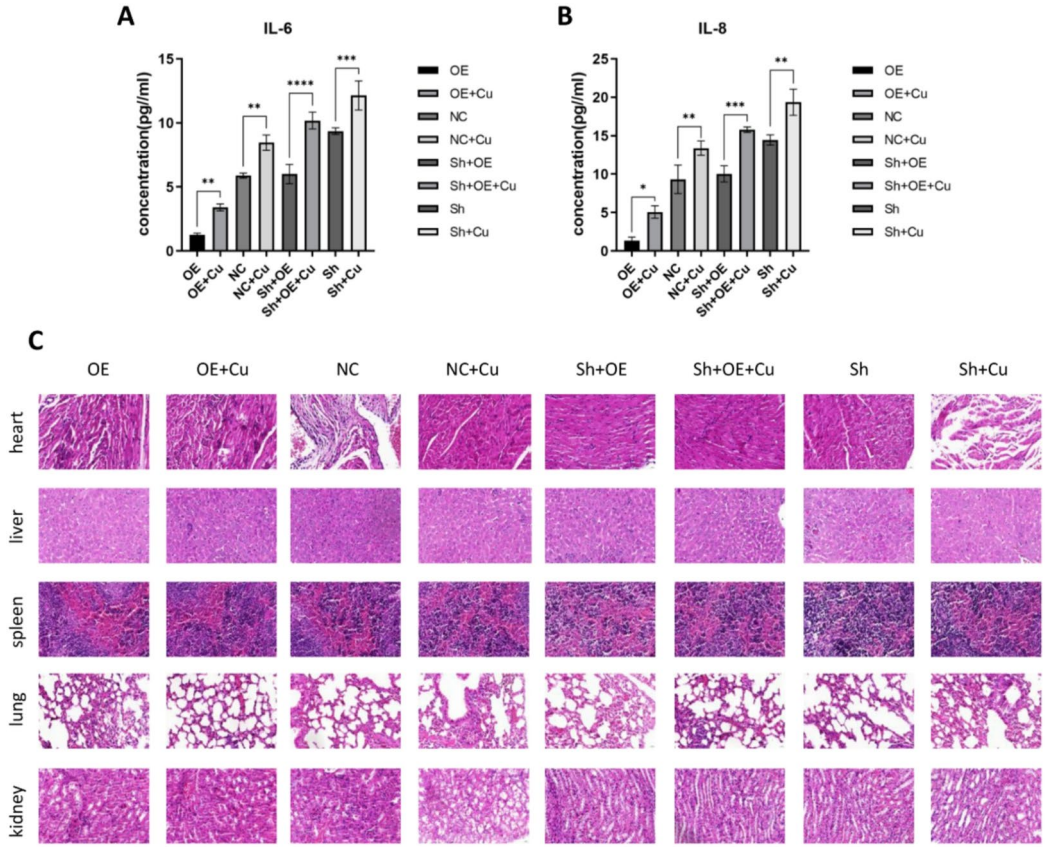

Fig. 6. Effect of RP11 on the immune microenvironment and drug safety evaluation of ES-Cu. (**A**) IL-6 content of each group. (**B**) IL-8 content of each group. (**C**) HE staining of heart, liver, spleen, lung and kidney sections from the mice. (*$P < 0.05$; **$P < 0.01$; ***$P < 0.001$; ****$P < 0.0001$). Data are presented as mean ± SD with 95% confidence intervals for pairwise differences; Bonferroni post-hoc correction was applied and adjusted *P* values are indicated in the figure.

copper probes and mitochondrial ultrastructure observations in organoid and PDX models to clarify the true contribution of copper death in the body.

From the perspective of immunity, the leakage of mtDNA and ATP accompanying copper death can activate the STING-NF-κB pathway, driving the maturation of DCs and the infiltration of $CD8^+$ T cells[29,30]. This study revealed that IL-6 and IL-8 were upregulated after RP11 was knocked down, suggesting that the RP11-FDX1 axis affects immune cell chemotaxis by regulating the inflammatory network. Consistent with recent reports, cuproptosis activation concurrently increases PD-L1 and IL-6/IL-8 transcription via NF-κB signaling. Thus, our observed parallel rise in cuproptosis proteins and these immune markers supports a mechanistic coupling between copper-death induction and local inflammatory modulation[27]. Whether this translates to altered DC or $CD8^+$ T-cell numbers requires immunocompetent or humanized models. These cytokine changes reflect local inflammatory modulation only and cannot be equated with adaptive immune escape.

From a clinical translational perspective, CA125 shows insufficient early sensitivity[31]. However, the stability and detectability of RP11 in serum exosomes have been preliminarily verified, laying the foundation for its use as a noninvasive dynamic monitoring indicator[32–34]. ES-Cu, as a copper ion carrier that has entered a phase III trial by the FDA, has redevelopment value because of its demonstrated survival benefits when combined with paclitaxel in melanoma[35,36]; this study provides a mechanistic basis for its "repositioning" in HGSOC. Moreover, the establishment of the expression threshold of RP11 and the dose-effect curve of ES-Cu will determine the stratification strategy for patients. When RP11 is combined with PARP inhibitors, PD-1 antibodies or antiangiogenic drugs, the high-expression subgroup of RP11 may have synergistic effects due to its "copper death sensitivity", whereas the low-expression subgroup needs to avoid the additional toxicity caused by excessive copper ion levels[37,38].

In conclusion, the RP11-FDX1-copper death axis not only fills the research gap in the lncRNA regulation of copper homeostasis in HGSOC but also provides a druggable intervention point for "nonmutation-driven" drug resistance. With the maturity of copper metabolism probes, copper death real-time imaging, and liquid biopsy technologies, RP11 is expected to become a companion diagnostic marker, and ES-Cu may become a precise second-line treatment option for platinum-resistant HGSOC.

Conclusions

This study systematically elucidates the oncogenic role of the long noncoding RNA RP11-199F11.2 in HGSOC: it is associated with reduced FDX1 protein levels and limited copper-death activity, thereby promoting cancer proliferation and modulating local inflammatory cytokines. The four-level evidence chain of clinical, cellular, animal and pharmacological studies consistently indicates that high expression of RP11 predicts a poor prognosis, whereas the copper ion carrier ES-Cu can reverse the FDX1 downregulation mediated by RP11, reverse copper death and significantly inhibit cancers, with controllable toxicity. Therefore, RP11 can serve as a prognostic biomarker, and ES-Cu provides a precise combined copper death induction treatment strategy for RP11-positive patients, laying a theoretical and practical foundation for overcoming the treatment bottleneck of HGSOC.

Data availability

All the data generated or analysed during this study are included in this published article.

Received: 14 August 2025; Accepted: 13 November 2025
Published online: 24 November 2025

References

1. Hong, M. K. & Ding, D. C. Early diagnosis of ovarian cancer: A comprehensive review of the advances, challenges, and future directions. *Diagnostics (Basel).* https://doi.org/10.3390/diagnostics15040406 (2025).
2. Kahn, R. et al. Ten-year conditional probability of survival for patients with ovarian cancer: A new metric tailored to Long-term survivors. *Gynecol. Oncol.* **169**, 85–90. https://doi.org/10.1016/j.ygyno.2022.11.030 (2023).
3. Momenimovahed, Z., Tiznobaik, A., Taheri, S. & Salehiniya, H. Ovarian cancer in the world: Epidemiology and risk factors. *Int. J. Women's Health* **11**, 287–299. https://doi.org/10.2147/ijwh.S197604 (2019).
4. van Baal, J. et al. The effect of adjuvant chemotherapy on survival in patients with FIGO stage I high-grade serous ovarian cancer. *Gynecol. Oncol.* **153**, 562–567. https://doi.org/10.1016/j.ygyno.2019.03.257 (2019).
5. Tan, Y. T. et al. LncRNA-mediated posttranslational modifications and reprogramming of energy metabolism in cancer. *Cancer Commun. (Lond.)* **41**, 109–120. https://doi.org/10.1002/cac2.12108 (2021).
6. Wu, Y., Wen, X., Xia, Y., Yu, X. & Lou, Y. LncRNAs and regulated cell death in tumor cells. *Front. Oncol.* **13**, 1170336. https://doi.org/10.3389/fonc.2023.1170336 (2023).
7. Wu, Y. et al. m(6)A-induced lncRNA RP11 triggers the dissemination of colorectal cancer cells via upregulation of Zeb1. *Mol. Cancer* **18**, 87. https://doi.org/10.1186/s12943-019-1014-2 (2019).
8. Pan, C. et al. Cuproptosis: Mechanisms, biological significance, and advances in disease treatmen—A systematic review. *CNS Neurosci. Ther.* **30**, e70039. https://doi.org/10.1111/cns.70039 (2024).
9. Kuang, J. et al. Electron paramagnetic resonance insights into direct electron transfer between FDX1 and elesclomol-Cu(2+) complex in cuproptosis. *Chemistry* https://doi.org/10.1002/chem.202501145 (2025).
10. Ren, Z. et al. Cu(OH)(2) nanopesticide induced liver dysfunction in mice by targeting lipoylated tricarboxylic acid cycle proteins via ferredoxin 1. *J. Hazard Mater.* **494**, 138403. https://doi.org/10.1016/j.jhazmat.2025.138403 (2025).
11. Lin, C. H. et al. Protein lipoylation: Mitochondria, cuproptosis, and beyond. *Trends Biochem. Sci.* **49**, 729–744. https://doi.org/10.1016/j.tibs.2024.04.002 (2024).
12. Xie, J. et al. Involvement of copper in cell death and cancer. *Apoptosis* **30**, 488–505. https://doi.org/10.1007/s10495-024-02059-9 (2025).
13. Sun, B. et al. FDX1 downregulation activates mitophagy and the PI3K/AKT signaling pathway to promote hepatocellular carcinoma progression by inducing ROS production. *Redox Biol.* **75**, 103302. https://doi.org/10.1016/j.redox.2024.103302 (2024).
14. Luo, Y. et al. Copper(II)-based nano-regulator correlates cuproptosis burst and sequential immunogenic cell death for synergistic cancer immunotherapy. *Biomater. Res.* **28**, 0039. https://doi.org/10.34133/bmr.0039 (2024).
15. Zafar, H. et al. Biomimetic gold nanocages incorporating copper-human serum albumin for tumor immunotherapy via cuproptosis-lactate regulation. *J. Control Release* **372**, 446–466. https://doi.org/10.1016/j.jconrel.2024.06.059 (2024).
16. Jiang, A. et al. Copper death inducer, FDX1, as a prognostic biomarker reshaping tumor immunity in clear cell renal cell carcinoma. *Cells* https://doi.org/10.3390/cells12030349 (2023).
17. Conforti, R. A., Delsouc, M. B., Zorychta, E., Telleria, C. M. & Casais, M. Copper in gynecological diseases. *Int. J. Mol. Sci.* https://doi.org/10.3390/ijms242417578 (2023).
18. Kelliher, L. & Lengyel, E. Understanding long-term survival of patients with ovarian cancer—The tumor microenvironment comes to the forefront. *Cancer Res.* **83**, 1383–1385. https://doi.org/10.1158/0008-5472.Can-23-0333 (2023).
19. Gao, J. et al. Combination treatment with cisplatin, paclitaxel and olaparib has synergistic and dose reduction potential in ovarian cancer cells. *Exp. Ther. Med.* **22**, 935. https://doi.org/10.3892/etm.2021.10367 (2021).
20. Ranasinghe, R., Mathai, M. L. & Zulli, A. Cisplatin for cancer therapy and overcoming chemoresistance. *Heliyon* **8**, e10608. https://doi.org/10.1016/j.heliyon.2022.e10608 (2022).
21. Tendulkar, S. & Dodamani, S. Chemoresistance in ovarian cancer: Prospects for new drugs. *Anticancer Agents Med. Chem.* **21**, 668–678. https://doi.org/10.2174/1871520620666200908104835 (2021).
22. Tufail, M., Jiang, C. H. & Li, N. Immune evasion in cancer: Mechanisms and cutting-edge therapeutic approaches. *Signal Transduct. Target Ther.* **10**, 227. https://doi.org/10.1038/s41392-025-02280-1 (2025).
23. Lyu, Y., Wang, T., Huang, S. & Zhang, Z. Mitochondrial damage-associated molecular patterns and metabolism in the regulation of innate immunity. *J. Innate Immun.* **15**, 665–679. https://doi.org/10.1159/000533602 (2023).
24. Xiao, C. et al. Prognostic and immunological role of cuproptosis-related protein FDX1 in pan-cancer. *Front. Genet.* **13**, 962028. https://doi.org/10.3389/fgene.2022.962028 (2022).
25. Qian, S., Liu, J., Liao, W. & Wang, F. METTL3 promotes non-small-cell lung cancer growth and metastasis by inhibiting FDX1 through copper death-associated pri-miR-21-5p maturation. *Epigenomics* **15**, 1237–1255. https://doi.org/10.2217/epi-2023-0230 (2023).
26. Tang, D., Chen, X. & Kroemer, G. Cuproptosis: A copper-triggered modality of mitochondrial cell death. *Cell Res.* **32**, 417–418. https://doi.org/10.1038/s41422-022-00653-7 (2022).
27. Wang, X., Zhou, M., Liu, Y. & Si, Z. Cope with copper: From copper linked mechanisms to copper-based clinical cancer therapies. *Cancer Lett.* **561**, 216157. https://doi.org/10.1016/j.canlet.2023.216157 (2023).
28. Zhang, X. et al. Copper-mediated novel cell death pathway in tumor cells and implications for innovative cancer therapies. *Biomed. Pharmacother.* **168**, 115730. https://doi.org/10.1016/j.biopha.2023.115730 (2023).
29. Bryant, J. D., Lei, Y., VanPortfliet, J. J., Winters, A. D. & West, A. P. Assessing mitochondrial DNA release into the cytosol and subsequent activation of innate immune-related pathways in mammalian cells. *Curr. Protoc.* **2**, e372. https://doi.org/10.1002/cpz1.372 (2022).

30. Xia, L., Yan, X. & Zhang, H. Mitochondrial DNA-activated cGAS-STING pathway in cancer: Mechanisms and therapeutic implications. *Biochim. Biophys. Acta Rev. Cancer* **1880**, 189249. https://doi.org/10.1016/j.bbcan.2024.189249 (2025).
31. Kaaks, R. et al. A prospective study consortium for the discovery and validation of early detection markers for ovarian cancer—Baseline findings for CA125. *Clin. Cancer Res.* **31**, 2441–2453. https://doi.org/10.1158/1078-0432.Ccr-24-1845 (2025).
32. Huang, X. et al. RNA sequencing of plasma exosomes revealed novel functional long noncoding RNAs in hepatocellular carcinoma. *Cancer Sci.* **111**, 3338–3349. https://doi.org/10.1111/cas.14516 (2020).
33. Zhao, L. et al. Clinical significance of a new early diagnostic model for bladder cancer based on genome-wide microarray profiling of serum exosomal lncRNAs. *Int. Urol. Nephrol.* **57**, 1771–1783. https://doi.org/10.1007/s11255-024-04360-7 (2025).
34. Abd El Gwad, A. et al. Role of exosomal competing endogenous RNA in patients with hepatocellular carcinoma. *J. Cell Biochem.* **119**, 8600–8610. https://doi.org/10.1002/jcb.27109 (2018).
35. Wang, Q. et al. Elesclomol-copper nanoparticles overcome multidrug resistance in cancer cells. *ACS Appl. Mater. Interfaces* **16**, 13509–13524. https://doi.org/10.1021/acsami.3c17792 (2024).
36. Deng, S. et al. SB226, an inhibitor of tubulin polymerization, inhibits paclitaxel-resistant melanoma growth and spontaneous metastasis. *Cancer Lett.* **555**, 216046. https://doi.org/10.1016/j.canlet.2022.216046 (2023).
37. Wu, Z. et al. The synergistic effect of PARP inhibitors and immune checkpoint inhibitors. *Clin. Med. Insights Oncol.* **15**, 1179554921996288. https://doi.org/10.1177/1179554921996288 (2021).
38. Song, H. et al. Integrated analysis of pseudogene RP11–564D11.3 expression and its potential roles in hepatocellular carcinoma. *Epigenomics* **11**, 267–280. https://doi.org/10.2217/epi-2018-0152 (2019).

Acknowledgements
We are grateful to the funding agencies and all the researchers who contributed to this research.

Author contributions
Conceptualization, Shishi Xu, Linping Wang, Yingying Wu and Yanhui Lou; data curation, Shishi Xu, Linping Wang and Yingying Wu.; methodology, Shishi Xu, Linping Wang, Yingying Wu and Yanhui Lou; validation, Shishi Xu, Yingying Wu and Yanhui Lou; formal analysis, Shishi Xu, Linping Wang and Yingying Wu; resources, Yufang Xia, Lingzhi Wang, Xiao Yu, Xin Sun and Yanhui Lou; writing—original draft preparation, Shishi Xu.; writing—review and editing, Shishi Xu, Yufang Xia, Lingzhi Wang, Xiao Yu, Xin Sun and Yanhui Lou. All the authors have read and agreed to the published version of the manuscript.

Funding
This research was partially funded by a grant from the Shinan District Science and Technology Program in Qingdao, Shandong Province, China (grant no. 2022–2–006-YY). This research was also supported by the China Health and Medical Development Foundation.

Declarations

Competing interests
The authors declare no competing interests.

Ethics approval and consent to participate
All experimental protocols involving animals were approved by the Animal Experiment Ethics Review Committee of the Affiliated Hospital of Qingdao University (Approval No. AHQU-MAL20230616), and protocols involving human tissues were approved by the Medical Ethics Committee of the same institution (Approval No. QYFY WZLL 30704). All procedures were conducted in accordance with the Declaration of Helsinki and institutional guidelines, and performed in compliance with relevant regulations and ethical standards. Informed consent was obtained from all the subjects involved in the study. Written informed consent was obtained from the patients to publish this paper.

Additional information
Supplementary Information The online version contains supplementary material available at https://doi.org/10.1038/s41598-025-29080-5.

Correspondence and requests for materials should be addressed to Y.L.